Available online at www.sciencedirect.com
SCIENCE DIRECT®
Coordination Chemistry Reviews 249 (2005) 1830–1840
COORDINATION CHEMISTRY REVIEWS
www.elsevier.com/locate/ccr

Review

Temperature- and photo-induced phase transition in rubidium manganese hexacyanoferrate

Shin-ichi Ohkoshi [a,b,*], Hiroko Tokoro [a], Kazuhito Hashimoto [a,*]

[a] *Department of Applied Chemistry, School of Engineering, The University of Tokyo, 7-3-1, Hongo, Bunkyo-ku, Tokyo 113-8656, Japan*
[b] *PRESTO, JST, 4-1-8 Honcho Kawaguchi, Saitama, Japan*

Received 16 June 2004; accepted 8 November 2004
Available online 12 April 2005

Contents

Abstract

This article describes a temperature- and photo-induced phase transition in rubidium manganese hexacyanoferrate, $RbMn[Fe(CN)_6]$. This compound displays a drop in the magnetic susceptibility at 225 K ($=T_{1/2\downarrow}$) and an abrupt increase in the magnetic susceptibility at 300 K ($=T_{1/2\uparrow}$) in the cooling and warming processes, respectively. This phase transition is accompanied by a structural change from cubic ($F\bar{4}3m$) to tetragonal ($I\bar{4}m2$). The high-temperature (HT) and low-temperature (LT) phases are composed of $Mn^{II}(S=\frac{2}{5})$—NC—$Fe^{III}(S=\frac{1}{2})$ and $Mn^{III}(S=2)$—NC—$Fe^{II}(S=0)$, respectively. A metal-to-metal charge transfer from Mn^{II} to Fe^{III} and a Jahn–Teller distortion of the produced Mn^{III} ion cause this phenomenon. The magnetic transition entropy and enthalpy of the LT phase indicate that this phase shows a three-dimensional Heisenberg-type ferromagnetic lattice for the Mn^{III} sites with a T_c of 11.0 K, which is due to a valence delocalization mechanism. Ferromagnetic magnetization of LT phase in $Rb_{0.91}Mn_{1.05}[Fe(CN)_6]\cdot 0.6H_2O$ is reduced by irradiation with only one-shot of laser pulse and the quantum yield is above one and reaches 4.5. This photomagnetic effect is caused by a photo-induced phase transition from the LT phase to the HT phase.

Keywords: Charge transfer; Jahn–Teller effect; Ferromagnetism; Photo-induced phase transition; Photomagnetism

* Corresponding authors. Tel.: +81 3 5841 7248; fax: +81 3 5841 1142.
E-mail addresses: ohkoshi@light.t.u-tokyo.ac.jp (S. Ohkoshi), hashimoto@light.t.u-tokyo.ac.jp (K. Hashimoto).

0010-8545/$ – see front matter © 2004 Elsevier B.V. All rights reserved.
doi:10.1016/j.ccr.2004.11.015

1. Introduction

Studies that are related to a thermal phase transition and a photo-induced phase transition are extensively investigated in solid-state chemistry [1–4]. Thermal phase transition phenomena are observed in spin crossover or intramolecular electron transfer. In a spin crossover complex, a transition metal ion can be in either the low-spin or the high-spin state depending on the strength of the ligand field. When the thermal energy is close to the exchange energy that corresponds to the crossover, a spin transition occurs between the two spin states. This phenomenon is observed in octahedral coordinate iron transition metal complexes, e.g., $[Fe^{II}(NCX)_2(phen)_2]$ (X = S or Se; phen = 1,10-phenanthroline) [5] and $[Fe^{II}(2\text{-pic})_3]X_2$ (2-pic = 2-aminomethylpyridine; X = Cl, Br, I) [6]. Charge-transfer phase transitions have been observed in mixed-valence complexes [7–20], e.g., $[M^{III}{}_2M^{II}O(O_2C_2H_3)_6L_3]$ (M = Fe, Mn; L = H_2O, pyridine) [13–15] and $M(dta)_4I$ (M = Ni, Pt; dta = dithioacetato) [19,20]. Charge-transfer phase transitions that accompany spin crossovers have also been reported, e.g., $Co(py_2X)(3,6\text{-DBQ})_2$ (X = O, S, Se) [21] and $Na_{0.4}Co_{1.3}[Fe(CN)_6]\cdot 4.9H_2O$ [22,23]. A thermal phase transition often accompanies a thermal hysteresis loop [21–23], which is related to the cooperativity of the corresponding system. The cooperativity in a metal complex assembly is due to the interaction between a metal ion and lattice strain, e.g., an electron–phonon coupling [24], a Jahn–Teller distortion [25–27], and an elastic interaction [28–31]. Cyano-bridged metal assemblies such as hexacyanometalate- [4,32–64] and octacyanometalate-based magnets [64–76] are suitable for observing a thermal phase transition since they are mixed-valence compounds that have a strong cooperativity due to the CN ligand bridges.

Photo-induced phase transition effects have been also extensively studied in a variety of systems [60–63,70–72,77–83], e.g., cyanometalate-based magnets [60–63,70–72,77,78], organic-based magnets [79], spin crossover complexes [80,81], and diluted magnetic semiconductors [82]. Various theoretical analyses of photo-induced phase transitions have also been reported [30,84–87]. To date, we have demonstrated photomagnetic effects such as photo-induced magnetization and the photo-induced magnetic pole inversion, with cyano-briged bimetallic assemblies [60–62,70–72]. One possible method for achieving optical control of magnetization is to change the electron spin state of a magnetic material. For example, if photo-irradiation varies the oxidation numbers of transition metal ions within a magnetic material, its magnetization will be controlled. The bistability of the electronic states is also indispensable for observing photo-induced persistent magnetization since the energy barrier between these bistable states can maintain the photo-produced state even after photo-irradiation is stopped.

From this viewpoint, Prussian blue analogs are an attractive system due to their high T_c values [37,42]. In particular, Verdaguer and co-workers reported that $V^{II}[Cr^{III}(CN)]_{0.86}\cdot 2.8H_2O$ exhibits a T_c value of 315 K [40]. Successively, Girolami et al. and Miller et al. reported crystalline $K^IV^{II}[Cr^{III}(CN)_6]$ with T_c = 103 °C and amorphous $K^I_{0.058}V^{II/III}[Cr^{III}(CN)_6]_{0.79}(SO_4)_{0.058}\cdot 0.93H_2O$ with T_c = 99 °C powder, respectively [44,45]. In multi-metal Prussian blue analogs, the rational design of magnets based on the molecular-field theory is possible for the following reasons: (1) metal substitutions induce only small changes in the lattice constant and (2) superexchange interactions are only essentially effective between the nearest neighbor metal ions [46]. For example, we have designed a novel type of magnet that exhibits two compensation temperatures with the system of $(Ni^{II}_{0.22}Mn^{II}_{0.60}Fe^{II}_{0.18})_{1.5}[Cr^{III}(CN)_6]\cdot 7.5H_2O$, i.e., the spontaneous magnetization changes sign twice as the temperature is varied [49]. In this review, we show the temperature-induced phase transition and photo-induced demagnetization of ferromagnetic $RbMn[Fe(CN)_6]$ complex.

2. Preparation

Rubidium manganese hexacyanoferrate was prepared by reacting an aqueous solution (0.1 mol dm^{-3}) of $MnCl_2$ with a mixed aqueous solution of RbCl (1 mol dm^{-3}) and $K_3[Fe(CN)_6]$ (0.1 mol dm^{-3}) to yield a precipitate. The precipitate was filtered, dried, and yielded a powdered sample. The prepared compound was a light brown powder and elemental analyses for Rb, Mn, and Fe indicated that the precipitate obtained had a formula of $RbMn[Fe(CN)_6]$ (Calcd.: Rb, 24.26; Mn, 15.59; Fe, 15.85%; Found: Rb, 24.25; Mn, 15.95; Fe, 15.35%). The 1:1:1 ratio of Rb:Mn:Fe allowed the Mn ions to coordinate six cyanonitrogens. Consequently the network does not contain water molecules as shown in Fig. 1. Scanning electron microscope images showed that the powdered obtained sample was composed of cubic microcrystals that were 2.1 ± 1.1 μm. For the study of photo-induced phase transition, the sample was prepared by reacting an aqueous solution (0.1 mol dm^{-3}) of $MnCl_2$ with a mixed aqueous solution of RbCl (0.5 mol dm^{-3})

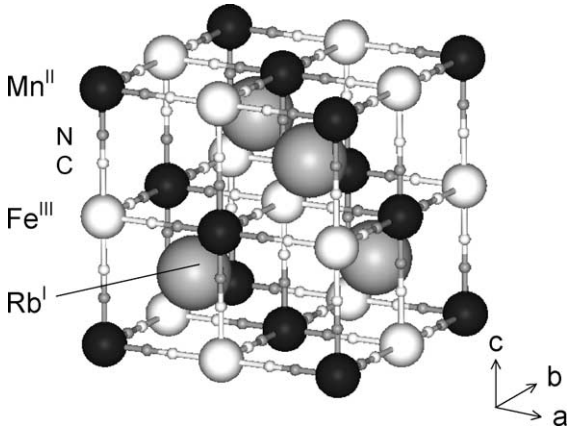

Fig. 1. Schematic structure of $Rb^IMn^{II}[Fe^{III}(CN)_6]$. Large gray circle is Rb^I ion, middle black circle is Mn^{II} ion, middle white circle is Fe^{III} ion, small white circle is C atom, and small gray circle is N atom.

and $K_3[Fe(CN)_6]$ (0.1 mol dm^{-3}). Elemental analyses for Rb, Mn, and Fe showed that the formula for the precipitate used in the photo-induced phase transition study was $Rb_{0.91}Mn_{1.05}[Fe(CN)6]\cdot 0.6H_2O$: Calcd.: Rb, 21.63; Mn, 16.09; Fe, 15.62%; Found: Rb, 21.18; Mn, 16.12; Fe, 15.24%.

3. Temperature-induced phase transition

3.1. Phase transition in magnetic susceptibility

Fig. 2 shows the product of the molar magnetic susceptibility (χ_M) and the temperature (T) versus T plots of $RbMn[Fe(CN)_6]$. The $\chi_M T$ value in the high-temperature (HT) phase is 4.67 cm^3 K mol^{-1} at 330 K, but cooling the sample at a cooling rate of 0.5 K min^{-1} decreases the $\chi_M T$ value around 235 K and at $T = 180$ K in the low-temperature (LT) phase reaches 3.19 cm^3 K mol^{-1}. Conversely, as the sample in the LT phase is warmed at a heating rate of 0.5 K min^{-1}, the $\chi_M T$ value suddenly increases near 285 K and reaches the HT phase value at 325 K. The transition temperatures from HT to LT ($T_{1/2\downarrow}$) and from LT to HT ($T_{1/2\uparrow}$) are 225 and 300 K, respectively, and the width of the thermal hysteresis loop ($\Delta T = T_{1/2\uparrow} - T_{1/2\downarrow}$) is 75 K. This temperature-induced phase transition is repeatedly observed.

3.2. Electronic states of high-temperature phase and low-temperature phase

X-ray photoelectron spectroscopy (XPS) spectra of $K^I_3[Fe^{III}(CN)_6]$, $K^I_4[Fe^{II}(CN)_6]$ and the HT and LT phases were measured. In the HT phase, the Fe $2p_{3/2}$ and Mn $2p_{3/2}$ electron binding energies are 710.1 and 641.8 eV, respectively, and in the LT phase, the Fe $2p_{3/2}$ and Mn $2p_{3/2}$ electron binding energies are 708.8 and 642.5 eV, respectively. The observed Fe $2p_{3/2}$ electron binding energy of 710.1 eV in the HT phase corresponds to that of 710.0 eV for Fe^{III} in $K^I_3[Fe^{III}(CN)_6]$. In contrast, Fe $2p_{3/2}$ binding energy of 708.8 eV in the LT phase is close to that of 709.1 eV for Fe^{II} in $K^I_4[Fe^{II}(CN)_6]$. The shift of the Mn $2p_{3/2}$ binding energy from the HT to the LT phases suggests that the oxidation number of the Mn ion increases from II to III.

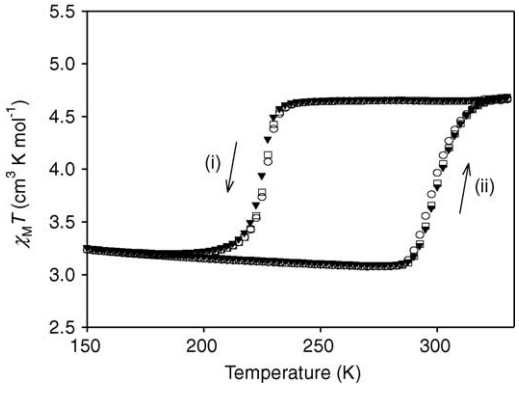

Fig. 2. The observed $\chi_M T$–T plots in the cooling (i) and warming (ii) processes with the first measurement (◯), second measurement (□), and third measurement (▼).

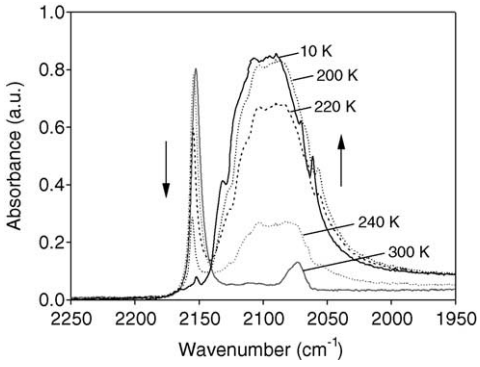

Fig. 3. Temperature dependence of the CN stretching frequencies in the IR spectra with decreasing temperature.

The infrared (IR) spectra are recorded over a temperature range between 300 and 10 K. Fig. 3 shows the CN^- stretching frequencies at 300, 240, 220, 200, and 10 K. At 300 K, a sharp CN^- peak is observed at 2152 cm^{-1} (linewidth = 9 cm^{-1}) and as the temperature decreases, the intensity of this peak decreases. Near 220 K a new broad peak appears at 2095 cm^{-1} (linewidth = 65 cm^{-1}). These IR changes are in the same temperature range of the phase transition in the $\chi_M T$–T plots. The CN stretching peak at 2152 cm^{-1} in the HT phase is due to the CN ligand bridged to Fe^{III} and Mn^{II} ions (Fe^{III}–CN–Mn^{II}). In contrast, the broad CN stretching peak at 2095 cm^{-1} in the LT phase is assigned to the CN ligand bridged to Fe^{II} and Mn^{III} ions (Fe^{III}–CN–Mn^{II}).

These XPS and IR spectra show that valence states for Mn and Fe ions in the HT phase are $Mn^{II}(d^5)$ and $Fe^{III}(d^5)$, respectively, and those in the LT phase are $Mn^{III}(d^4)$ and $Fe^{II}(d^6)$, respectively. The drop in the $\chi_M T$ value at $T_{1/2\downarrow}$ implies that the electronic states of the HT and LT phases are $Mn^{II}(d^5;\ S = \frac{5}{2})$–NC–$Fe^{III}(d^5;\ S = \frac{1}{2})$ and $Mn^{III}(d^4;\ S = 2)$–NC–$Fe^{II}(d^6;\ S = 0)$, respectively. These assignments are confirmed by Mn and Fe 3p–1s X-ray emission spectroscopy [88] and 1s X-ray absorption spectroscopy [89].

3.3. Structural change

Fig. 4 shows the powder X-ray diffraction (XRD) patterns as the temperature decreased from 300, 250, 240, 230, 220, 210, 200, 180, to 160 K. The diffraction pattern of the HT phase is consistent with a face-centered cubic ($F\bar{4}3m$) structure with a lattice constant of 10.533 Å (at 300 K). As the sample is cooled, the XRD peaks of the HT phase decrease and different peaks appear. The observed XRD pattern in the LT phase shows a tetragonal structure of $I\bar{4}m2$ with $a = b = 7.090$ Å and $c = 10.520$ Å (at 160 K), which corresponds to $a = b = 10.026$ Å and $c = 10.520$ Å in a cubic lattice. The unit cell volume of 1169 Å^3 in the HT phase is reduced about 10% to 1057 Å^3 in the LT phase and warm-

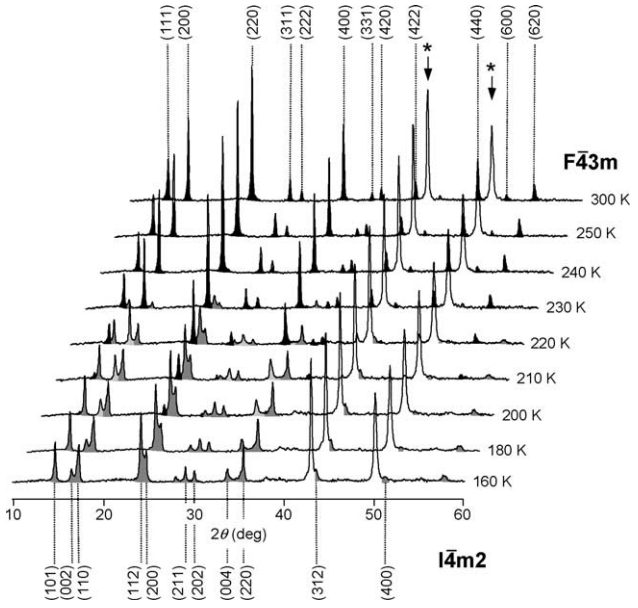

Fig. 4. Temperature dependences of XRD spectra. Black and gray peaks are the diffraction peaks of the HT and LT phases, respectively. The light gray peak is the overlapped peak from the HT and LT phases (* indicates Cu from the sample holder).

ing caused the tetragonal structure to return to the cubic one. This structural change from cubic to tetragonal in the XRD measurement is understood by the Mn^{III} Jahn–Teller transformation of the tetragonally octahedral elongation-type (B_{1g} oscillator mode) [90–95]. Synchrotron radiation X-ray powder structural analysis was used to determine the precise bond lengths of the LT phase, i.e., two-long and four-short Mn–N bond distances are 2.26(2) and 1.89(3) Å, respectively, and the two-short and four-long Fe–C bond distances are 1.89(2) and 2.00(3) Å, respectively [96]. Thus, the d-orbital symmetry of both metal ions in the LT phase is D_{4h} (a_{1g}, b_{1g}, b_{2g}, and e_g). Therefore, the precise electronic state of LT phase is $Mn^{III}(e_g^2 b_{2g}^1 a_{1g}^1; S=2)$–NC–$Fe^{II}(b_{2g}^2 e_g^4; S=0)$ (Fig. 5).

Fig. 6 shows the UV–vis absorption spectra of the HT and LT phases. In the HT phase, the absorption bands are approximately 410, 520, and 680 nm, while the band absorptions in LT phase are 540, 700, and 1100 nm. The visible absorption spectra can be explained based on the assigned electronic states of the HT and LT phases. Absorptions near 410 and 520 nm in the HT phase are due to a ligand-to-metal charge transfer of $[Fe^{III}(CN)_6]$ and d–d transition of Fe^{III} ($^2T_{2g} \rightarrow {}^4T_{1g}$), respectively [97]. In the LT phase, the absorptions around 540 nm ($^5B_{1g} \rightarrow {}^5B_{2g}$, ^5E_g) and 1100 nm

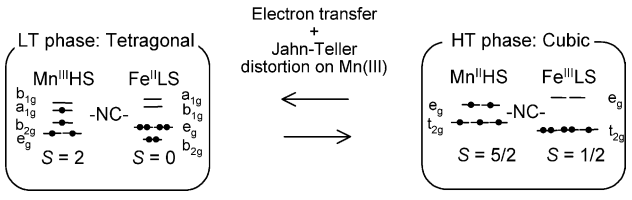

Fig. 5. Electronic states of the LT and HT phases.

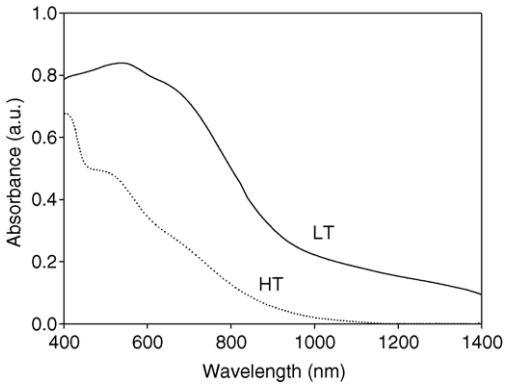

Fig. 6. UV–vis absorption spectra of the LT (solid line) and HT (dashed line) phases.

($^5B_{1g} \rightarrow {}^5A_{1g}$) are due to Jahn–Teller distorted Mn^{III} [90–95] and the broad absorption around 700 nm is from the metal-to-metal charge transfer band (intervalence transfer band) in the mixed-valence compound.

The molar heat capacity (C_p) of this compound between 2 and 320 K was measured (Fig. 7) and as the temperature increases, the heat capacity shows an anomalous peak in the temperature range of 290–300 K. A transition enthalpy (ΔH) of 1.7 kJ mol^{-1} and a transition entropy (ΔS) of 6 J K^{-1} mol^{-1} in this phase transition were obtained by eliminating the normal heat capacity of the LT phase.

3.4. Mechanism

Prussian blue analogs are class II mixed-valence compounds. This system is described by two parabolic potential-energy curves due to valence isomers in the nuclear coordinates of the coupled vibrational mode [7–12,16–18]. When these two vibronic states interact, the ground state surface has two minima in the vibrational coordinates. In the present system, the Mn^{III}–Fe^{II} vibronic state is a ground state at $T = 0$ K in the vibrational coordinates (mixed-valency mode) (black curve in Fig. 8(a)). Moreover, in this situation, Mn^{III} causes Jahn–Teller distortion, and then the energy of the Mn^{III}–Fe^{II} has two minima described

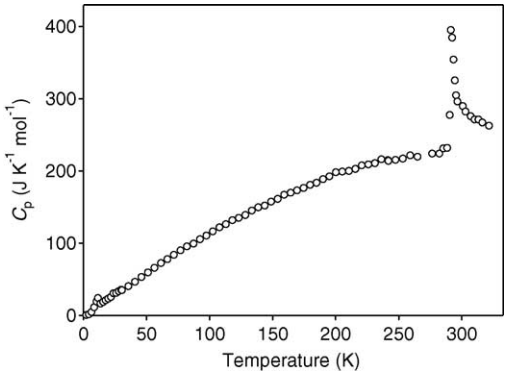

Fig. 7. C_p vs. T plots with increasing temperature.

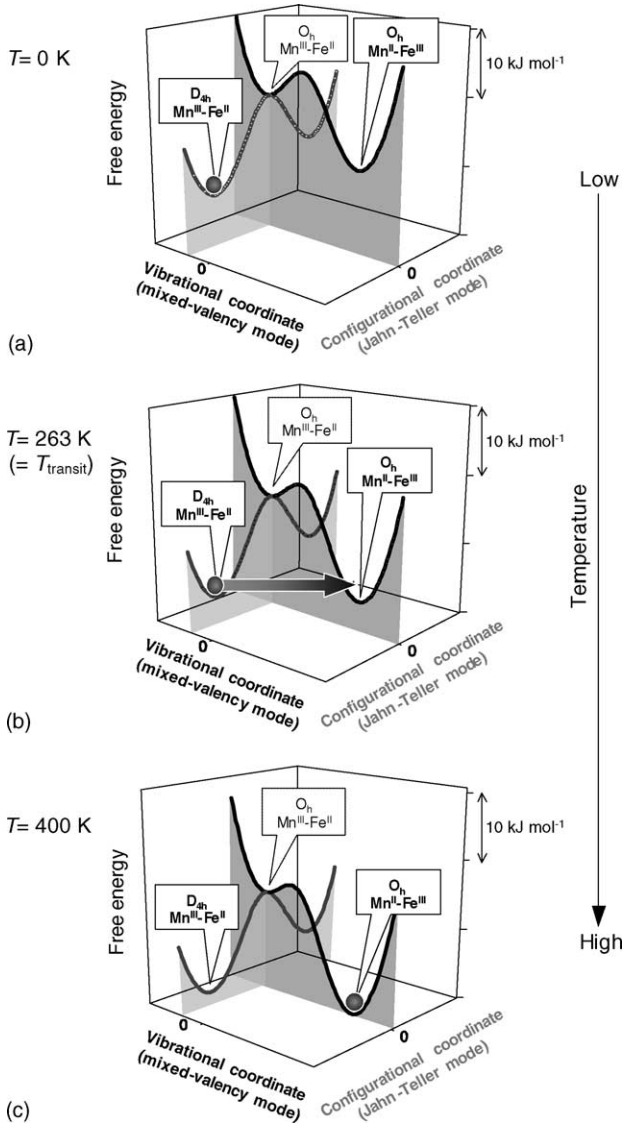

Fig. 8. The schematic free energy surfaces of this system in mixed-valence (black curve) and Jahn–Teller (gray curve) modes: (a) the ground state is Mn^{III}—Fe^{II} and the meta-stable state is Mn^{II}—Fe^{III} at $T = 0$ K, (b) $T = 263$ K ($=T_{transit}$), (c) the ground state is Mn^{II}—Fe^{III} and meta-stable state is Mn^{III}—Fe^{II} at $T = 400$ K. Each curve is calculated based on Eq. (1). Gray spheres indicate population.

in the configurational coordinates (Jahn–Teller mode) (gray curve in Fig. 8(a)). In the present system, Mn^{III} ion shows an elongation-type Jahn–Teller distortion. These potential surfaces change as the temperature increases, which cause a phase transition. To explain the obtained results, the free energy changes of the HT and LT phases are analyzed. The LT and HT phases consist of $D_{4h}Mn^{III}(^5B_{1g})$–$D_{4h}Fe^{II}(^1A_{1g})$ and $O_hMn^{II}(^6A_{1g})$–$O_hFe^{III}(^2T_{2g})$, respectively. The entropies due to the spin-multiplicities lead to a crossover from LT to HT phases with increasing temperature. The free energies of the LT phase (G_{LT}) and HT phase (G_{HT}) depend on the temperature as described in the following equation:

$$G_i = H_i - S_iT \quad (i = \mathrm{LT},\ \mathrm{HT}) \tag{1}$$

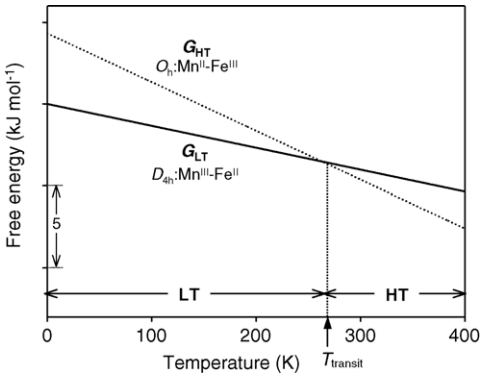

Fig. 9. Temperature dependence of the free energy for the HT (dotted line) and LT (solid line) phases based on Eq. (1) with $\Delta H = 4.3\,\mathrm{kJ\,mol^{-1}}$, $S_{LT} = 13.4$, and $S_{HT} = 29.8\,\mathrm{J\,K^{-1}\,mol^{-1}}$.

Since the LT phase has a 5-fold ($=5 \times 1$) degeneracy and the HT phase has a 36-fold ($=6 \times 6$) degeneracy, their entropies (S_{LT} and S_{HT}) are $S_{LT} = R\ln 5$ and $S_{HT} = R\ln 36$, respectively. Thus, the ΔS in this phase transition is $R\ln(36/5) = 16.4\,\mathrm{J\,K^{-1}\,mol^{-1}}$. From Eq. (1) the transition temperature ($T_{transit}$) of the phase transition can be obtained by $\Delta H/\Delta S$. In this system, $T_{transit}$ is defined as $T_{transit} = (T_{1/2\downarrow} + T_{1/2\uparrow})/2 = 263$ K. Using $T_{transit} = 263$ K and $\Delta S = 16.4\,\mathrm{J\,K^{-1}\,mol^{-1}}$, ΔH value of $4.3\,\mathrm{kJ\,mol^{-1}}$ is obtained. Fig. 9 shows the calculated temperature dependence of G_{LT} and G_{HT} based on Eq. (1) with $\Delta S = 16.4\,\mathrm{J\,K^{-1}\,mol^{-1}}$ and $\Delta H = 4.3\,\mathrm{kJ\,mol^{-1}}$. G_{LT} and G_{HT} change as the temperature increases and a phase transition occurs at $T_{transit}$. In addition, Fig. 8(b) and (c) show the surfaces of G_{LT} and G_{HT} in the vibrational (mixed-valency mode) and configurational coordinates (Jahn–Teller mode) at each temperature. Heat capacity measurements show $\Delta S = 6\,\mathrm{J\,K^{-1}\,mol^{-1}}$ and $\Delta H = 1.7\,\mathrm{kJ\,mol^{-1}}$. These experimental values are smaller than the theoretical values, which may be due to a small orbital contribution to the entropy of Fe^{III} in the HT phase. The extended X-ray absorption fine structure data of the HT phase shows a small distortion in the octahedral coordinates of metal ions, which is due to a small contribution from the LT phase [89]. In this situation, $^2T_{2g}$ of Fe^{III} is reduced to $^2B_{2g}$, and then ΔS and ΔH are changed to $R\ln(12/5) = 7.28\,\mathrm{J\,K^{-1}\,mol^{-1}}$ and $1.9\,\mathrm{kJ\,mol^{-1}}$, respectively, which is close to the experimental values.

4. Ferromagnetism of the low-temperature phase

4.1. Magnetic ordering and specific heat

As the LT phase is cooled to a very low temperature under an external magnetic field of 10 G, it exhibits spontaneous magnetization with a Curie temperature (T_c) of 11.3 K (Fig. 10). The magnetization as a function of the external magnetic field at 3 K indicates that the saturated magnetization (M_s) value is 3.6 μ_B (Fig. 11(a)) and the coercive field (H_c) value is 1050 G (Fig. 11(b)). The χ_M^{-1}–T plots of the para-

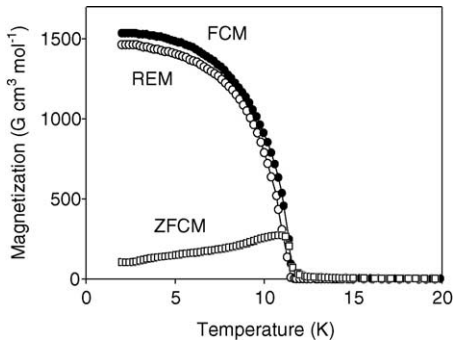

Fig. 10. Magnetization vs. temperature plots of the LT phase by SQUID measurement: (●) field-cooled magnetization (FCM) at B_0 = 10 G, (□) zero field-cooled magnetization (ZFCM) at B_0 = 10 G, and (◯) remnant magnetization (REM) data for $Rb^{I}Mn^{III}[Fe^{II}(CN)_6]$.

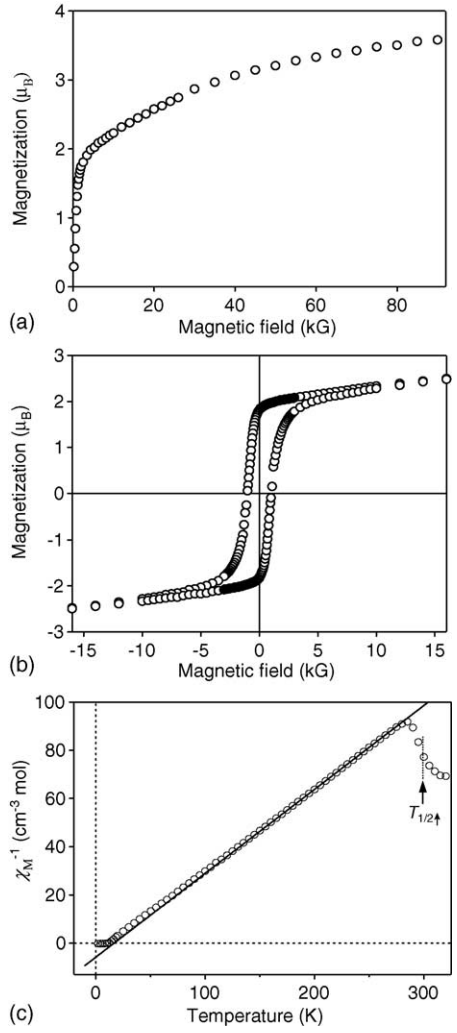

Fig. 11. (a) Magnetization vs. external magnetic field plots of the LT phase at 3 K. (b) Magnetic hysteresis loop of the LT phase at 3 K. (c) The observed χ_M^{-1}–T plots. The data between 150 and 270 K is fitted to Curie–Weiss plots (—).

magnetic LT phase show positive Weiss temperatures (Θ) between 12 and 15 K, which are obtained by extrapolating the data in the temperature region of 30–270 and 150–270 K, respectively (Fig. 11(c)).

The C_p value in low temperature region gradually increases with temperature and reaches a maximum, 27.1 J K^{-1} mol^{-1} at 11.0 K (denoted here as T_p), as shown in Fig. 12. Then it drops suddenly to 17.5 J K^{-1} mol^{-1}, and increases gradually. The dependence of the C_p values on the external magnetic field is shown in Fig. 13, where the T_p peaks shift to a higher temperature as the external magnetic field increases: T_p = 11.0 K (B_0 = 0 T), 11.0 K (0.05 T), 11.2 K

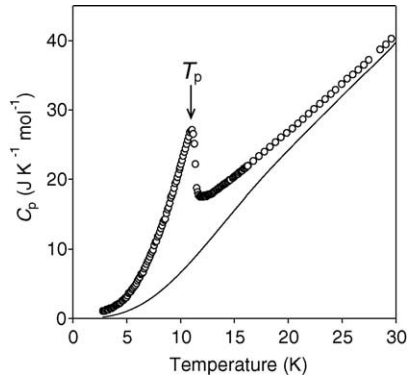

Fig. 12. Plots of C_p vs. T in a zero external magnetic field: (◯) experimental and (—) derived C_{lat} curve based on Eq. (3).

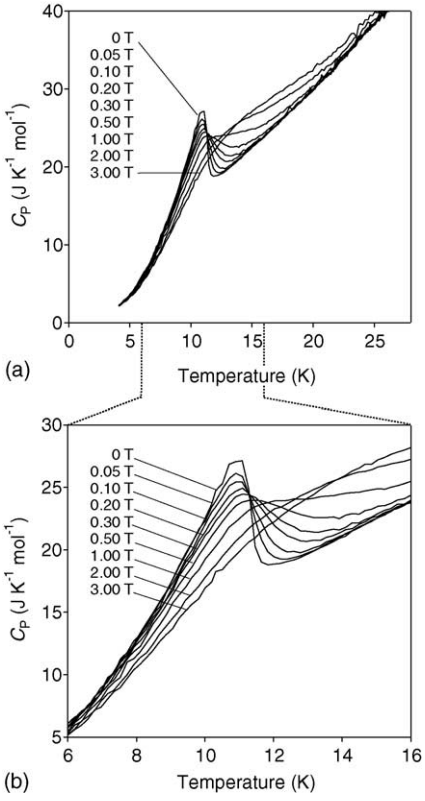

Fig. 13. (a) Plots of C_p vs. T in the presence of an external magnetic field, B_0; (b) enlarged plots of (a).

(0.10 T), 11.3 K (0.20 T), 11.4 K (0.30 T), 11.5 K (0.50 T), 11.9 K (1.00 T), 13.8 K (2.00 T), and 15.2 K (3.00 T).

4.2. Entropy and enthalpy of magnetic phase transition

Since $RbMn[Fe(CN)_6]$ is an insulating magnetic system, the C_p value is described as a sum of the contributions from lattice vibration, C_{lat}, short-range magnetic ordering, C_{short}, and long-range magnetic ordering, C_{long}:

$$C_p = C_{lat} + C_{short} + C_{long} \quad (2)$$

C_{lat} is described by a polynomial function of temperature with odd powers [98,99]:

$$C_{lat} = aT^3 + bT^5 + cT^7 + dT^9 + eT^{11} + \cdots \quad (3)$$

and C_{short} is described by AT^{-2} [100]. We fitted the C_p data in the region between 15 K (=1.4 × T_c) and 30 K (=2.7 × T_c) by the contributions of $C_{lat} + C_{short}$, using analyses reported in other systems [101,102]. The derived coefficients, including the estimated uncertainties (±7.4%) from the experiment (±7.0%) and curve fitting (±2.3%), are as follows: $a = 8.08 \times 10^{-3}$ J K^{-4} mol^{-1}, $b = -2.10 \times 10^{-5}$ J K^{-6} mol^{-1}, $c = 2.56 \times 10^{-8}$ J K^{-8} mol^{-1}, $d = -1.18 \times 10^{-11}$ J K^{-10} mol^{-1}, and $A = 1130$ J K mol^{-1}. The solid line in Fig. 13 shows the C_{lat} curve. The magnetic specific heat, $C_{mag} = C_{short} + C_{long}$, is obtained by subtracting C_{lat} from C_p, as shown in Fig. 14. The magnetic transition entropy, ΔS_{mag}, and enthalpy, ΔH_{mag}, can be obtained from

$$\Delta S_{mag} = \int_0^T C_{mag}\, d\ln T \quad (4)$$

and

$$\Delta H_{mag} = \int_0^T C_{mag}\, dT \quad (5)$$

The estimated values of ΔS_{mag} and ΔH_{mag} for $Rb^{I}Mn^{III}[Fe^{II}(CN)_6]$ are 11.8 ± 0.9 J K^{-1} mol^{-1} and 125 ± 9 J mol^{-1}, respectively.

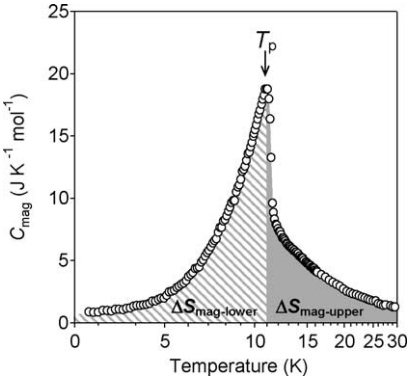

Fig. 14. Plots of C_{mag} vs. log T.

4.3. Type of long-range magnetic ordering and exchange coupling

Since the T_p value of 11.0 K agrees with the T_c value of 11.3 K derived from a SQUID measurement, the anomalous peak at T_p can be ascribed to a magnetic phase transition. The ΔS_{mag} value of 11.8 ± 0.9 J K^{-1} mol^{-1} is close to the value calculated for the ordering of magnetic spins on the Mn^{III} ($S = 2$) sites for $Rb^{I}Mn^{III}[Fe^{II}(CN)_6]$ given by $R\ln(2S + 1) = 13.4$ J K^{-1} mol^{-1}, where R is the gas constant. Thus, the origin of this magnetic phase transition is attributed to the long-range magnetic ordering of the Mn^{III} sites.

The temperature dispersion of ΔS_{mag} allows the dimensionality of magnetic ordering to be determined, i.e., two- or three-dimensional (2D or 3D) magnetic lattice. When the value of ΔS_{mag} is divided into two terms, such as the magnetic entropy values below T_p ($\Delta S_{mag\text{-}lower}$) and above T_p ($\Delta S_{mag\text{-}upper}$), the ratio of $\Delta S_{mag\text{-}lower}/\Delta S_{mag}$ for the magnetic lattices of the 3D Ising, 2D Ising, and 3D Heisenberg types are 81, 44, and 62%, respectively [103]. The ratio of $\Delta S_{mag\text{-}lower}/\Delta S_{mag}$ in the present system is 65(3)% (Fig. 14). Therefore, in this framework the magnetic ordering of the LT phase is most likely 3D Heisenberg-type magnetic ordering. Note that magnetic anisotropy should appear in this system since the crystal structure of the LT phase is tetragonal instead of cubic. This magnetic anisotropy may slightly influence the comparison between the observed value of ≈65% and the theoretical value of 62%.

Analyzing C_{mag} at very low temperatures using the spin-wave theory can determine if the long-range magnetic ordering of a target material is ferromagnetic or antiferromagnetic. The specific heat due to the spin-wave excitation, C_{SW}, is expressed by [104]:

$$C_{sw} = \alpha T^{d/n} \quad (6)$$

where d stands for the dimensionality of the magnetic lattice and n the exponent in the dispersion relationship: $n = 1$ for antiferromagnets and $n = 2$ for ferromagnets. We fitted the C_{mag} values in the region between 2.8 and 4.7 K to Eq. (6) (Fig. 15)

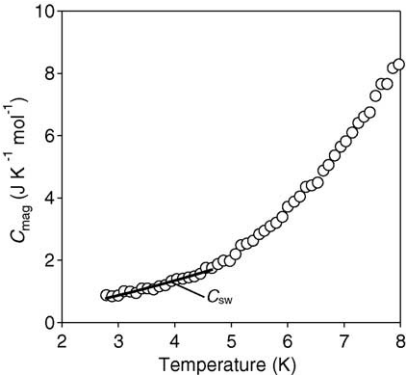

Fig. 15. Experimental plots of C_{mag} (◯) and the C_{SW} curve (—) calculated from the spin-wave theory for a 3D ferromagnet using Eq. (6) with $d/n = 1.51$ and $\alpha = 0.17$ J K$^{-5/2}$ mol^{-1}.

and the estimated the parameter of d/n is 1.51(11). This d/n value is consistent with that predicted for the magnetic ordering of the LT phase, i.e., the 3D ferromagnet, where $d = 3$ and $n = 2$. The observed shifts in the T_p values of the in-field C_p data, 11.0 K (0 T) → 15.2 K (3.00 T) displayed in Fig. 13, which also suggest ferromagnetic character. Since the shift in T_p to higher temperatures is characteristic of ferromagnetic transitions [105], the trend of the in-field C_p values observed in the present study gives direct evidence that the magnetic ordering of the LT phase is ferromagnetic.

Although diamagnetic Fe^{II} is bridged to Mn^{III} in an alternating fashion, this system shows a 3D Heisenberg-type ferromagnetic ordering. The exchange coupling constant, J, of this ferromagnet can be evaluated in the following manner. The α value derived from Eq. (6) is related to the J value. In C_{SW} for a 3D ferromagnet, the coefficient α is described by [106]:

$$\alpha = \frac{1}{\sqrt{2}} \frac{5R\zeta(5/2)\Gamma(5/2)}{16\pi^2 S^{3/2}} \left(\frac{k_B}{J}\right)^{3/2} \tag{7}$$

where ζ is the Riemann's zeta function, Γ the Euler's gamma function, and k_B the Boltzmann constant. Since the α value obtained from Eq. (6) is 0.17(1) J $K^{-5/2}$ mol^{-1}, the estimated J value based on Eq. (7) is +0.55(4) cm^{-1} ΔH_{mag} is also related to the J value in an extension of the molecular-field theory. In this treatment, ΔH_{mag} due to long-range magnetic ordering is expressed by

$$\frac{\Delta H_{mag}}{R} = \frac{S^2 z J}{k_B} \tag{8}$$

where the number of neighboring magnetic sites, z, is 6 in the present system. The estimated J value from Eq. (8), using $\Delta H_{mag} = 125 \pm 9$ J mol^{-1} is +0.44(3) cm^{-1}.

4.4. Mechanism

The application of the superexchange interaction mechanism to the present ferromagnetic ordering is difficult since the diamagnetic Fe^{II} sites are connected by paramagnetic Mn^{III} sites. One plausible mechanism is the valence delocalization mechanism, in which ferromagnetic coupling arises from the charge-transfer configuration [107]. Mayoh and Day explained the ferromagnetism of $Fe^{III}[Fe^{II}(CN)_6]_{0.75}\cdot 3.5H_2O$ by the ferromagnetic exchange interaction based on a partial delocalization of the electrons that occupy the $Fe^{II}t_{2g}$ orbitals next to the neighboring high-spin Fe^{III} sites [107]. Since Fe^{III} in Prussian blue is replaced with Mn^{III}, the same mechanism is feasible in our system. In fact, an intense intervalence transfer (IT) band of the LT phase has been observed at 700 nm and in the IT band of Prussian blue. In the valence delocalization mechanism, the T_c value is related to the valence delocalization coefficient of c as $T_c \propto c^4$. The c value is given by second-order perturbation theory as

$$c = \sum_{i=2,3} \left(\frac{\langle \psi_0 | H | \psi_i \rangle \langle \psi_1 | H | \psi_i \rangle}{(E_1 - E_0)(E_i - E_0)} \right) \tag{9}$$

where ψ_0, ψ_1, ψ_2, and ψ_3 are the ground (pure Mn^{III}–Fe^{II}) state and the charge-transfer configurations of $Fe^{II} \rightarrow Mn^{III}$, $Fe^{II} \rightarrow CN$, and $CN \rightarrow Mn^{III}$, respectively, and $E_0 - E_3$ are their energies. Mixing these excited charge-transfer configurations with the ground state causes the ferromagnetic exchange coupling. The J value of $\approx$+0.5 cm^{-1} in the present system is three times larger than that of +0.15 cm^{-1} in Prussian blue. This large J value means that $Rb^{I}Mn^{III}[Fe^{II}(CN)_6]$ has a large c value. Namely, the electrons on the Fe^{II} site are delocalized to the Mn^{III} site.

5. Photo-induced phase transition

5.1. One-shot-laser-pulse-induced demagnetization

The photomagnetic effect of the LT phase was investigated with $Rb_{0.91}Mn_{1.05}[Fe(CN)6]\cdot 0.6H_2O$ using SQUID magnetometer. The powder was spread on a commercial transparent adhesive tape and the sample was mounted on the straw of the sample rod. A pulsed Nd^{3+}; YAG laser (λ = 355, 532, and 1064 nm; pulse width: 6 ns) was guided by an optical fiber into the SQUID magnetometer. When the sample was irradiated by one-shot-laser-pulse with 532-nm laser light at 3 K, the magnetization decreased. Fig. 16(a) and (b), respectively, show the time- and temperature-dependences of magnetization for a sample irradiated with $P = 130$ mJ cm^{-2} $pulse^{-1}$. The photo-conversion increases with the laser power density (P), e.g., 7.7% ($P = 9.7$), 15% ($P = 15$), 54% ($P = 43$), and 88% ($P = 130$ mJ cm^{-2} $pulse^{-1}$). As shown in Fig. 17, a threshold in the laser power density (P_{th}) is observed when the P value is above 9.3 mJ cm^{-2} $pulse^{-1}$ and the magnetization value is reduced, however, in the case of $P < P_{th}$, the magnetization value did not change. The quantum yields (Φ) for the present photodemagnetization are above one, e.g., $\Phi = 2.8$ ($P = 9.7$), $\Phi = 3.6$ ($P = 15$), $\Phi = 4.5$ ($P = 43$), and $\Phi = 2.4$ ($P = 130$ mJ cm^{-2} $pulse^{-1}$). Annealing (3 K → 150 K → 3 K) with a relaxation temperature of 120 K returned the irradiated sample to the LT phase. In contrast, when the sample is irradiated with a laser pulse of 355 or 1064 nm, the photodemagnetization values are very small as shown in Fig. 17(a). In addition, the threshold excitation powers differed among the excitation lights (Fig. 17(b)). The P_{th} values at 355 and 1064 nm are 3.9 and 6.1 times as the P_{th} value at 532 nm, respectively, when their absorptions are equivalent. These differences indicate that the observed one-shot-laser-induced demagnetization phenomenon is not due to photo-thermal reaction, but the *photochemical reaction* via the photo-excited state. The optical absorption spectra indicate that the photo-excited state will be an

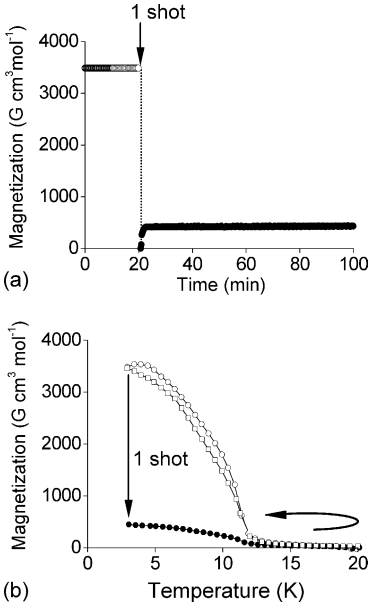

Fig. 16. (a) Magnetization vs. time plots for $Rb_{0.91}Mn_{1.05}[Fe(CN)_6]\cdot 0.6H_2O$ at 3 K in the field of $H = 200$ G before (◯) and after one-shot-laser-pulse irradiation (532 nm, 130 mJ cm^{-2} pulse^{-1}) (●). (b) Magnetization vs. temperature plots at $H = 200$ G before (◯) and after the one-shot-laser-pulse irradiation (●) and thermal treatment (□). Magnetic measurement sequence; 20 K → ◯ → 3 K (one-shot-laser-pulse irradiation) → ● → 150 K (thermal treatment) → □ → 3 K.

excited mixed-valence state between Fe^{III}–CN–Mn^{II} and the Fe^{III}–CN–Mn^{II}.

Fig. 18 shows the IR spectra before and after one-shot-laser-pulse irradiation (532 nm, $P = 14$ mJ cm^{-2} pulse^{-1}) at 8 K. After irradiation, the Fe^{III}–CN–Mn^{II} peak at 2095 cm^{-1} disappears and a sharp peak due to the Fe^{III}–CN–Mn^{II} peak at 2152 cm^{-1} simultaneously appears. Note that, in the case of $P < P_{th}$, the irradiation does not change the IR spectra. An annealing treatment (8 K → 150 K → 8 K) with a relaxation temperature of 120 K returned the IR spectrum of the irradiated sample to the LT phase. From these results, we conclude that the present photo-demagnetization is caused by the photo-induced phase transition from the LT phase to the HT phase.

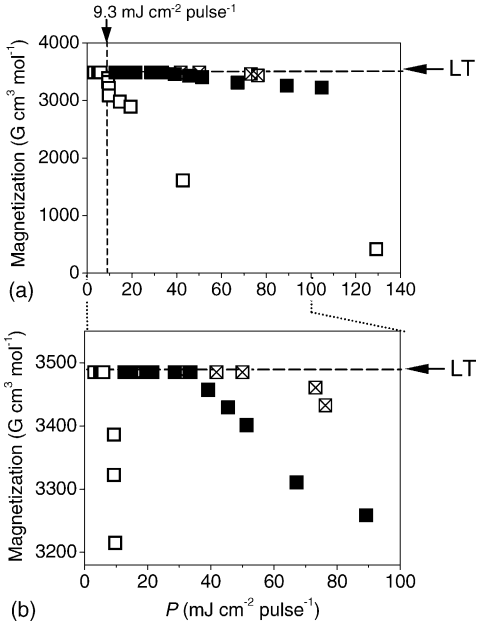

Fig. 17. (a) Laser power density (P) dependences of the one-shot-laser-pulse induced photodemagnetization phenomenon with irradiation of the 355 (■), 532 (□) and 1064 nm (□) at $H = 200$ G. (b) Enlarged plots of (a).

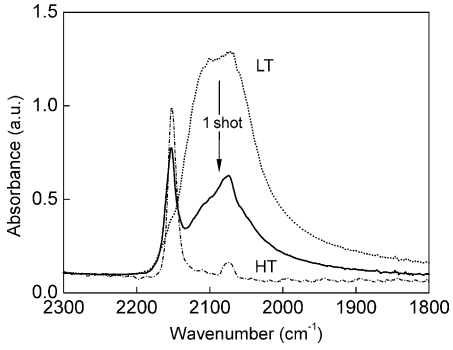

Fig. 18. IR spectra for $Rb_{0.91}Mn_{1.05}[Fe(CN)_6]\cdot 0.6H_2O$ at 8 K before (···) and after (—) one-shot-laser-pulse irradiation at 532 nm with 14 mJ cm^{-2} pulse^{-1}. HT phase at room temperature (- - -).

5.2. Mechanism

Rubidium manganese hexacyanoferrate exhibits a temperature-induced phase transition between the LT and HT phases. In such a material with a bistability, a ground state can be converted to a hidden substable state by the irradiation. Nasu et al. showed a simple scheme for a photo-induced phase transition using the adiabatic potential energy vs. order parameter (Fig. 19) [84,85]. In this scheme, the ground state is excited to the Franck–Condon state by irradiation. This Franck–Condon state proceeds to a hidden substable state through a structural change state or relaxes to the ground state. In our case, irradiating with pulsed-laser light excites the LT phase to a mixed-valence state between the Fe^{III}–CN–Mn^{II} and the Fe^{III}–CN–Mn^{II} states. This mixed-valence state proceeds to the HT phase or relaxes to the initial LT phase. The produced HT phase can be maintained in the low temperature range since it is sufficiently separated from the LT phase by the thermal energy (ΔG). In addition, when the P value is larger than P_{th}, the excited state proceeds to the photo-produced HT phase as shown by the solid arrow in Fig. 19. In contrast, when $P < P_{th}$, the excited state relaxes to the ground state as shown by the dotted arrow in Fig. 19. This threshold behavior in the photo-induced phase transition is observed in tetrathiafuluvalene-*p*-chloranil system. The mechanism of this system is understood by the bistable electronic model proposed by Koshino and Ogawa [108]. The observed threshold behavior in the present system is explained by a similar mechanism.

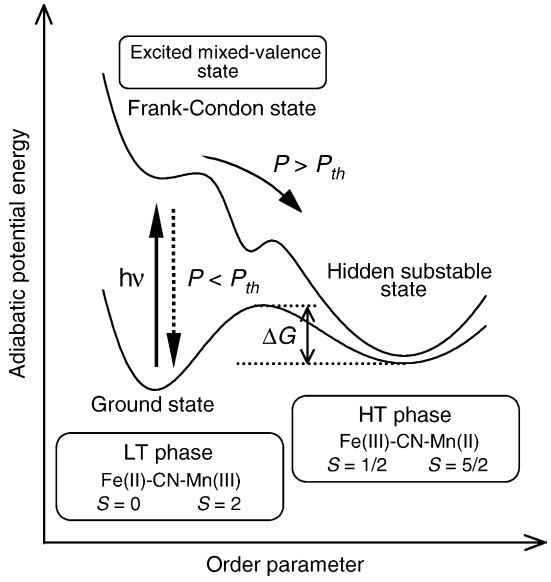

Fig. 19. Schematic illustration of the one-shot-laser-pulse-induced phase transition from the stable Fe^{III}—CN—Mn^{II} phase to the hidden substable Fe^{III}—CN—Mn^{II} phase.

6. Conclusion

In summary, a temperature-induced phase transition in RbMn[Fe(CN)6] ($T_{1/2\downarrow}$ = 225 K, $T_{1/2\uparrow}$ = 300 K) is observed with a large thermal hysteresis loop of 75 K. The charge transfer from Mn^{II} to Fe^{III} that accompanies the Jahn–Teller effect on the $Mn^{III}N_6$ moiety explains this phase transition. The magnetic coupling between the Mn^{III} spin sites in the LT phase is prevented by the diamagnetic Fe^{II} sites, but ferromagnetic ordering is achieved by the valence delocalization mechanism. With this system, the photo-induced phase transition from the LT to HT phase has also been observed. These temperature- and photo-induced phase transition phenomena are caused by: (1) the change in valence states on transition metal ions due to metal-to-metal charge-transfer and (2) the bistability due to the Jahn–Teller distortion of Mn^{III} ion.

References

[1] H.A. Goodwin, Coord. Chem. Rev. 18 (1976) 293.
[2] P. Gütlich, Struct. Bonding (Berlin) 44 (1981) 83.
[3] O. Kahn, Molecular Magnetism, VCH, New York, 1993.
[4] S. Ohkoshi, K. Hashimoto, J. Photochem. Photobiol. C 2 (2001) 71.
[5] J.F. Létard, P. Guionneau, E. Codjovi, O. Lavastre, G. Bravic, D. Chasseau, O. Kahn, J. Am. Chem. Soc. 119 (1997) 10861.
[6] G.A. Renovitch, W.A. Baker, J. Am. Chem. Soc. 89 (1967) 6377.
[7] M.B. Robin, P. Day, Adv. Inorg. Chem. Radiochem. 10 (1967) 247.
[8] N.S. Hush, Prog. Inorg. Chem. 8 (1967) 391.
[9] S.B. Piepho, E.R. Krausz, P.N. Schatz, J. Am. Chem. Soc. 10 (1978) 2996.
[10] D.B. Brown, Mixed Valence Compounds, NATO ASI, Reidel, Dordrecht, 1980.
[11] J.P. Launay, F. Babonneau, Chem. Phys. 67 (1982) 295.
[12] S.A. Borshch, I. Kotov, I.B. Bersuker, Chem. Phys. Lett. 89 (1982) 381.
[13] R.D. Cannon, L. Montri, D.B. Brown, K.M. Marshall, C.M. Elliot, J. Am. Chem. Soc. 106 (1984) 2591.
[14] M. Sorai, K. Kaji, D.N. Hendrickson, S.M. Oh, J. Am. Chem. Soc. 108 (1986) 702.
[15] H.J. Jang, J.B. Vincent, M. Nakano, C. Huffman, G. Christou, M. Sorai, R.J. Wittebort, D.N. Hendrickson, J. Am. Chem. Soc. 111 (1989) 7778.
[16] K. Prassides, Mixed Valency Systems, Applications in Chemistry, Physics and Biology, NATO ASI, Kluwer, Dordrecht, 1991.
[17] D.N. Hendrickson, Mixed Valency Systems, Applications in Chemistry, Physics and Biology, Kluwer, Boston, 1991.
[18] S.A. Borshch, K. Prassides, J. Phys. Chem. 100 (1996) 9348.
[19] H. Kitagawa, N. Onodera, T. Sonoyama, M. Yamamoto, T. Fukuwa, T. Mitani, M. Seto, Y.J. Maeda, J. Am. Chem. Soc. 121 (1999) 10068.
[20] H. Kitagawa, T. Mitani, Coord. Chem. Rev. 190 (1999) 1169.
[21] O.S. Jung, D.H. Jo, Y.A. Lee, B.J. Conklin, C.G. Pierpont, Inorg. Chem. 36 (1997) 19.
[22] O. Sato, Y. Einaga, T. Iyoda, A. Fujishima, K. Hashimoto, J. Phys. Chem. B 101 (1997) 3903.
[23] N. Shimamoto, S. Ohkoshi, O. Sato, K. Hashimoto, Inorg. Chem. 41 (2002) 678.
[24] R.J. Zimmermann, Phys. Chem. Solids 44 (1983) 151.
[25] T.J. Kambara, Phys. Soc. Jpn. 49 (1980) 1806.
[26] N. Sasaki, T.J. Kambara, Chem. Phys. 74 (1981) 3472.
[27] T.J. Kambara, Chem. Phys. 74 (1981) 4557.
[28] S. Ohnishi, S. Sugano, J. Phys. C 14 (1981) 39.
[29] H. Spiering, E. Meissner, H. Köppen, E.W. Müller, P. Gütlich, Chem. Phys. 68 (1982) 65.
[30] K. Boukheddaden, I. Shteto, B. Hôo, F. Varret, Phys. Rev. B 62 (2000) 14796.
[31] K. Boukheddaden, J. Linares, E. Codjovi, F. Varret, V. Niel, J.A. Real, J. Appl. Phys. 93 (2003) 7103.
[32] A. Ludi, H.U. Güdel, Struct. Bonding (Berlin) 14 (1973) 1.
[33] J.S. Miller, MRS Bull. 25 (2000) 60.
[34] K. Hashimoto, S. Ohkoshi, Phil. Trans. Roy. Soc. A 357 (1999) 2977.
[35] S. Ohkoshi, K. Hashimoto, Magneto-Optics, Springer Verlag, Berlin, 2000, pp. 243–267.
[36] S. Ohkoshi, K. Hashimoto, Electrochem. Soc. Interf. (2002) 34.
[37] T. Mallah, S. Thiébaut, M. Verdaguer, P. Veillet, Science 262 (1993) 1554.
[38] M. Verdaguer, T. Mallah, V. Gadet, I. Castro, C. Hélary, S. Thiébaut, P. Veillet, Conf. Coord. Chem. 14 (1993) 19.
[39] W.R. Entley, G.S. Girolami, Science 268 (1995) 397.
[40] S. Ferlay, T. Mallah, R. Ouahès, P. Veillet, M. Verdaguer, Nature 378 (1995) 701.
[41] W.E. Buschmann, S.C. Paulson, C.M. Wynn, M.A. Girtu, A.J. Epstein, H.S. White, J.S. Miller, Adv. Mater. 9 (1997) 645.
[42] M. Verdaguer, A. Bleuzen, C. Train, R. Garde, F. Fabrizi de Biani, C. Desplanches, Phil. Trans. Soc. London, Ser. A 357 (1999) 2959.
[43] M. Verdaguer, A. Bleuzen, V. Marvaud, J. Vaissermann, M. Seuleiman, C. Desplanches, A. Scuiller, C. Train, R. Garde, G. Gelly, C. Lomenech, I. Rosenman, P. Veillet, C. Cartier, F. Villain, Coord. Chem. Rev. 190 (1999) 1023.
[44] S.M. Holmes, G.S. Girolami, J. Am. Chem. Soc. 121 (1999) 5593.
[45] Ø. Hatlevik, W.E. Bushmann, J. Zhang, J.L. Manson, J.S. Miller, Adv. Mater. 11 (1999) 914.
[46] S. Ohkoshi, T. Iyoda, A. Fujishima, K. Hashimoto, Phys. Rev. B 56 (1997) 11642.
[47] S. Ohkoshi, O. Sato, T. Iyoda, A. Fujishima, K. Hashimoto, Inorg. Chem. 36 (1997) 268.
[48] S. Ohkoshi, A. Fujishima, K. Hashimoto, J. Am. Chem. Soc. 120 (1998) 5349.

[49] S. Ohkoshi, Y. Abe, A. Fujishima, K. Hashimoto, Phys. Rev. Lett. 82 (1999) 1285.
[50] S. Ohkoshi, K. Hashimoto, Chem. Phys. Lett. 314 (1999) 210.
[51] S. Ohkoshi, K. Hashimoto, Phys. Rev. B 60 (1999) 12820.
[52] S. Ohkoshi, K. Hashimoto, J. Am. Chem. Soc. 121 (1999) 10591.
[53] Z. Zhong, H. Seino, Y. Mizobe, M. Hidai, A. Fujishima, S. Ohkoshi, K. Hashimoto, J. Am. Chem. Soc. 122 (2000) 2952.
[54] S. Ohkoshi, M. Mizuno, G.J. Hung, K. Hashimoto, J. Phys. Chem. B 104 (2000) 9365.
[55] M. Mizuno, S. Ohkoshi, K. Hashimoto, Adv. Mater. 12 (2000) 1955.
[56] S. Ohkoshi, H. Tokoro, M. Utsunomiya, M. Mizuno, M. Abe, K. Hashimoto, J. Phys. Chem. B 106 (2002) 2423.
[57] K. Ikeda, S. Ohkoshi, K. Hashimoto, J. Appl. Phys. 93 (2003) 1371.
[58] Y. Sato, S. Ohkoshi, K. Arai, M. Tozawa, K. Hashimoto, J. Am. Chem. Soc. 125 (2003) 14590.
[59] H. Tokoro, S. Ohkoshi, T. Matsuda, T. Hozumi, K. Hashimoto, Chem. Phys. Lett. 388 (2004) 379.
[60] O. Sato, T. Iyoda, A. Fujishima, K. Hashimoto, Science 271 (1996) 49.
[61] S. Ohkoshi, S. Yorozu, O. Sato, T. Iyoda, A. Fujishima, K. Hashimoto, Appl. Phys. Lett. 70 (1997) 1040.
[62] Y. Sato, S. Ohkoshi, K. Hashimoto, J. Appl. Phys. 92 (2002) 4834.
[63] H. Tokoro, S. Ohkoshi, K. Hashimoto, Appl. Phys. Lett. 82 (2002) 1245.
[64] R. Garde, C. Desplanches, A. Bleuzen, P. Veillet, M. Verdaguer, Mol. Cryst. Mol. Liq. Cryst. 334 (1999) 587.
[65] J. Larionova, M. Gross, M. Pilkington, H. Andres, E.H. Stoeckli, H.U. Güdel, S. Decurtins, Angew. Chem., Int. Ed. Engl. 39 (2000) 1605.
[66] G. Rombaut, M. Verelst, S. Golhen, L. Ouahab, C. Mathoniere, O. Kahn, Inorg. Chem. 40 (2001) 1151.
[67] R. Podgajny, T. Korzeniak, M. Balanda, T. Wasiutynski, W. Errington, T.J. Kemp, N.W. Alcock, B. Sieklucka, Chem. Commun. 10 (2002) 1138.
[68] D. Li, S. Gao, L. Zheng, W. Tang, J. Chem. Soc., Dalton Trans. 12 (2002) 2805.
[69] Z.J. Zhong, H. Seino, Y. Mizobe, M. Hidai, M. Verdaguer, S. Ohkoshi, K. Hashimoto, Inorg. Chem. 39 (2000) 5095.
[70] S. Ohkoshi, N. Machida, Z.J. Zhong, K. Hashimoto, Synth. Met. 122 (2001) 523.
[71] T. Yokoyama, K. Okamoto, T. Ohta, S. Ohkoshi, K. Hashimoto, Phys. Rev. B 65 (2002) 64438.
[72] Y. Arimoto, S. Ohkoshi, Z.J. Zhong, H. Seino, Y. Mizobe, K. Hashimoto, J. Am. Chem. Soc. 125 (2003) 9240.
[73] S. Ohkoshi, Y. Arimoto, T. Hozumi, H. Seino, Y. Mizobe, K. Hashimoto, Chem. Commun. 22 (2003) 2772.
[74] S. Ohkoshi, T. Hozumi, K. Hashimoto, Phys. Rev. B 64 (2001) 132404.
[75] T. Hozumi, S. Ohkoshi, H. Seino, Y. Mizobe, K. Hashimoto, J. Phys. Chem. B 107 (2003) 11571.
[76] T. Kashiwagi, S. Ohkoshi, H. Seino, Y. Mizobe, K. Hashimoto, J. Am. Chem. Soc. 126 (2004) 5024.
[77] A. Bleuzen, C. Lomenech, V. Escax, F. Villain, F. Varret, C.C.D. Moulin, M. Verdaguer, J. Am. Chem. Soc. 122 (2000) 6648.
[78] D.A. Pejaković, J.L. Manson, J.S. Miller, A.J. Epstein, Phys. Rev. Lett. 85 (2000) 1994.
[79] D.A. Pejaković, C. Kitamura, J.S. Miller, A.J. Epstein, Phys. Rev. Lett. 88 (2002) 057202.
[80] P. Gütlich, A. Hauser, H. Spiering, Angew. Chem. Int. Ed. 33 (1994) 2024.
[81] J.F. Létard, J.A. Real, N. Moliner, A.B. Gaspar, L. Capes, O. Cador, O. Kahn, J. Am. Chem. Soc. 121 (1999) 10630.
[82] S. Koshihara, A. Oiwa, M. Hirasawa, S. Katsumoto, Y. Iye, C. Urano, H. Takagi, H. Munekata, Phys. Rev. Lett. 78 (1997) 4617.
[83] A.K. Giri, E.M. Kirkpatrick, P. Moongkhamklang, S.A. Majetich, V.G. Harris, Appl. Phys. Lett. 80 (2002) 2341.
[84] K. Nasu, Relaxations of Excited States and Photo-induced Structural Phase Transitions, Springer-Verlag, Berlin, 1997.
[85] K. Nasu, H. Ping, H. Mizouchi, J. Phys. Condens. Matter 13 (2001) 693.
[86] K. Iwano, Phys. Rev. B 61 (2000) 279.
[87] M. Nishino, S. Miyashita, Phys. Rev. B 63 (2001) 174404.
[88] H. Osawa, T. Iwazumi, H. Tokoro, S. Ohkoshi, K. Hashimoto, H. Shoji, E. Hirai, T. Nakamura, S. Nanao, Y. Isozumi, Solid State Commun. 125 (2003) 237.
[89] T. Yokoyama, H. Tokoro, S. Ohkoshi, K. Hashimoto, K. Okamoto, T. Ohta, Phys. Rev. B 66 (2002) 184111.
[90] S.T. Davis, P.J. Fackler, J.M. Weeks, Inorg. Chem. 7 (1968) 1994.
[91] M.D. Doddrell, R.M. Bendall, T.D. Pegg, C.P. Healy, K.A. Gregson, J. Am. Chem. Soc. 99 (1977) 1281.
[92] M. Gerloch, Inorg. Chem. 20 (1981) 638.
[93] R. Åkesson, M.G.L. Pettersson, M. Sandström, U.J. Wahlgren, Phys. Chem. 96 (1992) 150.
[94] S. Kück, S. Hartung, S. Hurling, K. Petermann, G. Huber, Phys. Rev. B 57 (1998) 2203.
[95] J. Krzystek, J. Telser, A.L. Pardi, P.D. Goldberg, M.B. Hoffman, C.L. Brunel, Inorg. Chem. 38 (1999) 6129.
[96] Y. Moritomo, K. Kato, A. Kuriki, M. Takata, M. Sakata, H. Tokoro, S. Ohkoshi, K. Hashimoto, J. Phys. Soc. Jpn. 71 (2002) 2078.
[97] S.C. Naiman, J. Chem. Phys. 35 (1961) 323.
[98] T. Matsumoto, Y. Miyazaki, A.S. Albrecht, C.P. Landee, M.M. Turnbull, M. Sorai, J. Phys. Chem. B 104 (2000) 9993.
[99] T. Nakamoto, Y. Miyazaki, M. Itoi, Y. Ono, N. Kojima, M. Sorai, Angew. Chem. Int. Ed. 40 (2001) 4716.
[100] H.M.J. Blöte, Physica B 79 (1975) 427.
[101] T. Matsumoto, Y. Miyazaki, A.S. Albrecht, C.P. Landee, M.M. Turnbull, M. Sorai, J. Phys. Chem. B 104 (2000) 9993.
[102] C.M. Ramsey, B. Cage, P. Nguyen, K.A. Abboud, N.S. Dalal, Chem. Mater. 15 (2003) 92.
[103] R.L. Carlin, Magnetochemistry, Springer, New York, 1986.
[104] L.J. de Jongh, A.R. Miedema, Adv. Phys. 23 (1974) 1.
[105] M.A. Subramanian, A.P. Ramirez, W.J. Marshall, Phys. Rev. Lett. 82 (1999) 1558.
[106] N. Ohmae, A. Kajiwara, Y. Miyazaki, M. Kamachi, M. Sorai, Thermochim. Acta 267 (1995) 435.
[107] B. Mayoh, P. Day, J. Chem. Soc. Dalton 15 (1976) 1483.
[108] K. Koshino, T. Ogawa, Phys. Rev. B 61 (2000) 12101.